Viral life cycles captured in three-dimensions with electron microscopy tomography

Chi-yu Fu and Johnson E Johnson

Viruses hijack host-cell functions and optimize them for viral replication causing a severe threat to human health. However, viruses are also tools to understand cell biology and they may be effective reagents in nanomedicine. Studies from the molecular to cellular levels are aimed at understanding the details of viral life cycles and the underlying virus–host interactions. Recent developments in electron microscopy tomography allow viral and cellular events to be observed in fine structural detail in three-dimensions. By combining high-resolution structures of individual proteins and macrocomplexes obtained by crystallography and electron cryomicroscopy and image reconstruction with reconstructions performed on subtomographic volumes, electron tomography has advanced the structural and mechanistic understanding of virus infections both *in vitro* and in host cells.

Address
Department of Molecular Biology, The Scripps Research Institute, La Jolla, CA 92037, USA

Corresponding author: Johnson, Johnson E (jackj@scripps.edu)

Introduction

Electron microscopy has been widely applied to visualize the ultrastructures of cells and tissues and to reveal morphological changes caused by virus infection. Electron tomography (ET) extends imaging from two-dimensions (2D) to three-dimensions (3D) where the specimens are tilted typically ±60° or 70° along an axis perpendicular to the electron beam. A series 2D projection images are collected at 1–2° intervals and aligned with each other and then back-projected to generate 3D images [1,2].

In order to minimize the inelastic scattering and to obtain sufficient signal-to-noise ratio (SNR) of the images, cells or tissues are fixed, traditionally with chemicals, and sectioned to about 50–250 nm in thickness. An alternative to chemical fixation is high pressure freezing in combination with freeze substitution, providing better preservation of the ultrastructures [3]. Electron cryotomography (cryotomog) eliminates fixation entirely and approaches resolution in the 4-nm range. Samples are preserved in vitreous ice by flash freezing and then examined with low electron doses while maintaining cryoconditions. Cryotomog minimizes artifacts introduced during sample fixation, dehydration and staining, and therefore preserves structures in a virtually native state. Cryotomog can be applied to small prokaryotic cells without sectioning or to regions of eukaryotic cells that are flattened [1,2]. Analysis of larger cells requires, technically challenging, cryosectioning [4].

ET requires only the combination of different views of the same entity with no averaging of different objects, making it a superior method to analyze pleiomorphic objects. Some medically important viruses (e.g. influenza and HIV) are pleiomorphic, prohibiting the use of crystallography or electron cryomicroscopy with image reconstruction (cryo-EM). ET characterizations of purified viruses revealed the structural complexity of HIV, Influenza, Hanta and Herpes etc. [5–8]. On the other hand, ET can identify asymmetric structural changes inside symmetric objects. The method allowed visualization of the specialized DNA packaging vertex in the icosahedral HSV capsid [9,10], the geometry of the poliovirus capsid releasing its genome [11], the structural changes of the tail machinery of Epsilon15 upon injecting its genome [12], or the conformational changes of hemagglutinin molecules of influenza virus upon fusing with liposomes [13]. A significant issue affecting the images generated by ET is the 'missing wedge' of data caused by the 140° physical limit associated with the tilts. This causes significant artifacts in certain, predictable, regions of the image [1]. The problem can be reduced with multiple tilt axes and, if applicable, performing sub tomographic volume averaging. The latter can significantly improve the resolution if objects are sufficiently uniform to be averaged. The growing applications of ET to characterize virus structures and various stages of the virus life cycle *in vitro* and *in vivo* have been well documented in several reviews [14–16]. Here we emphasize recently published work on viruses. Tomographic studies of viruses from 2010 to date are listed in the Table 1.

Applications of electron tomography to study viral life cycles

HIV

ET has contributed significantly to our understanding of the complicated HIV assembly process as well as its

Table 1

Tomography studies of viruses from 2010 to date

Family	Virus	Methods	Studies	Ref
Cystoviridae	φ12	Cryotomog	Architectures of viral surface complexes responsible for host-cell attachment	[57]
		Subtomo average		
Cystovirida	φ6	Cryotomog	Random occupancy of RNA polymerase and packaging NTPase on φ6 procapsids	[58]
		Subtomo average		
Podoviridae	P-SSP7	Cryotomog	Structural changes in podoviruses associated with release of its genome into Prochlorococcus	[59]
		Subtomo average Cellular cryotomog		
Podoviridae	BPP-1	Cryo-EM	Structure of tropism-switching Bordetella bacteriophage	[60]
		Cryotomog Subtomo average		
Rudiviridae	Sulfolobus turreted icosahedral virus	Whole cell cryotomog	Viral life cycle in host sulfolobus cells	[36]
		Subtomo average		
Bunyaviridae	Hantaan virus	Cryo-EM	Architectures of envelop glycoprotein spike complexes on viruses	[8]
		Cryotomog Subtomo average		
Bunyaviridae	Hanta viruses	Cryotomog Subtomo average	Architectures of Tula hantavirus	[5]
Coronaviridae	Corona Viruses	Subtomo average	Structural analysis of M protein in relation to virus assembly and morphology	[61]
Flaviviridae	Dengue virus	Cellular ET	Viral replication in a human endothelial cell line	[62]
Flaviviridae	Dengue virus	Cellular ET	Dengue virus-induced autophagosomes and changes in endomembrane ultrastructure	[62]
herpesviridae	Gammaherpes Viruses	Cellular ET	Gammaherpesvirus life cycle in host cells	[30••]
Orthomyxo-viridae	Influenza virus	Cryotomog	Architecture of a nascent viral fusion pore	[13]
Picornaviridae	Polio virus	Cryo-EM Cryotomog Subtomo average	Architectures of the virus releasing the genome	[11]
Retroviridae	HIV-1	Cryotomog Subtomo average	Structural analysis of HIV-1 maturation	[21]
		Cellular cryotomog Subtomo average	Architectures of viral particles at native budding sites	[23••]
		Cryotomog	Maturation inhibitor bevirimat functions as stabilizing the immature gag lattice	[63]
		Subtomo average Cellular ET	HIV transfers at the virological synapse between dendritic cells and T cells	[24]
	HIV-1	Cryotomog	Strain-dependent variation in architectures of trimeric envelope glycoproteins	[64]
	Simian immunodeficiency virus HIV	Subtomo average Cryotomog	Conserved and variable features of gag structure and arrangement in immature retrovirus particles	[65]
	Mason-Pfizer monkey virus Rous Sarcoma Virus	Subtomo average		
	Rous sarcoma virus	Cryotomog	Tomography characterization of morphogenic mutations on capsid assembly	[66]
Reoviridae	Cytoplasmic polyhedrosis virus	ET	Architectures of viral particles embedded inside a crystalline protein occlusion body called polyhedra	[67]
Togaviridae	Semliki forest virus	Cellular ET	Structural evidence of glycoprotein assembly in cellular membrane compartments prior to viral budding	[68]
Togaviridae	Rubella virus	Cellular ET	Structures of Rubella virus factories	[69]

maturation and cellular egress. The viral polyprotein Gag assembles on the interior cell membrane and recruits other viral components and the RNA genome, as well as the host ESCRT machinery necessary for the sub-sequent viral budding. The immature form of the virion undergoes series of proteolytic cleavages by the viral protease and converts into an infectious mature particle. While the virions are pleomorphic, repeating patterns in

the particle surface lattice were characterized and enhanced by sub tomographic averaging [17]. This allowed the Gag lattice in the immature virions to be reconstructed to 17 Å and revealed that the incomplete hexagonal lattice packing creates curvature through symmetry defects with irregular shape and size. Upon proteolytic cleavage of Gag the lattice maintains its largely hexagonal organization but loses its defects, and rearranges to incorporate pentameric CA capsomers for curvature, creating the characteristic cone shape of the mature capsid core [18–20]. By studying Gag mutations abolishing cleavage at individual or multiple cleavage sites, the structural transformations corresponding to the maturation process were revealed in significant detail [21].

HIV assembly and release were also examined at their budding sites during cellular egress. The budding process is initiated by Gag assembly and completed in an ESCRT-dependent manner, initially forming an incomplete ∼2/3 Gag sphere [22]. The cryotomog studies of intact plunge-frozen human cells concluded that the gag lattice in budding sites was indistinguishable from that of

the released immature virion (Figure 1) [23••]. The control of proteolytic maturation is critical, because its loss led to the formation of aberrant particles.

Cell to cell contacts and the distribution of HIV virions at the synapses formed between mature dendritic cells and T cells were also revealed in 3D [24]. The T cells were embraced by sheet-like membrane extensions derived from the dendritic cells, which create shielded virological synapses. The unique aspects of cell–cell transmission in the receptor-dependent viral transfers were visualized in the secluded synapses. The distribution of glycoprotein spikes on the viral surface in contacts with cells during entry was characterized in earlier studies [25].

Filoviruses
Marburg and Ebola viruses cause severe hemorrhagic fever with high mortality rates in humans. The release of the highly infectious filamentous particles was captured in 3D [26•]. The budding process is initiated with the lateral association of the viral nucleocapsid with the plasma membrane. A rapid envelopment started at one end of the nucleocapsid followed by a scission process

Figure 1

Current Opinion in Virology
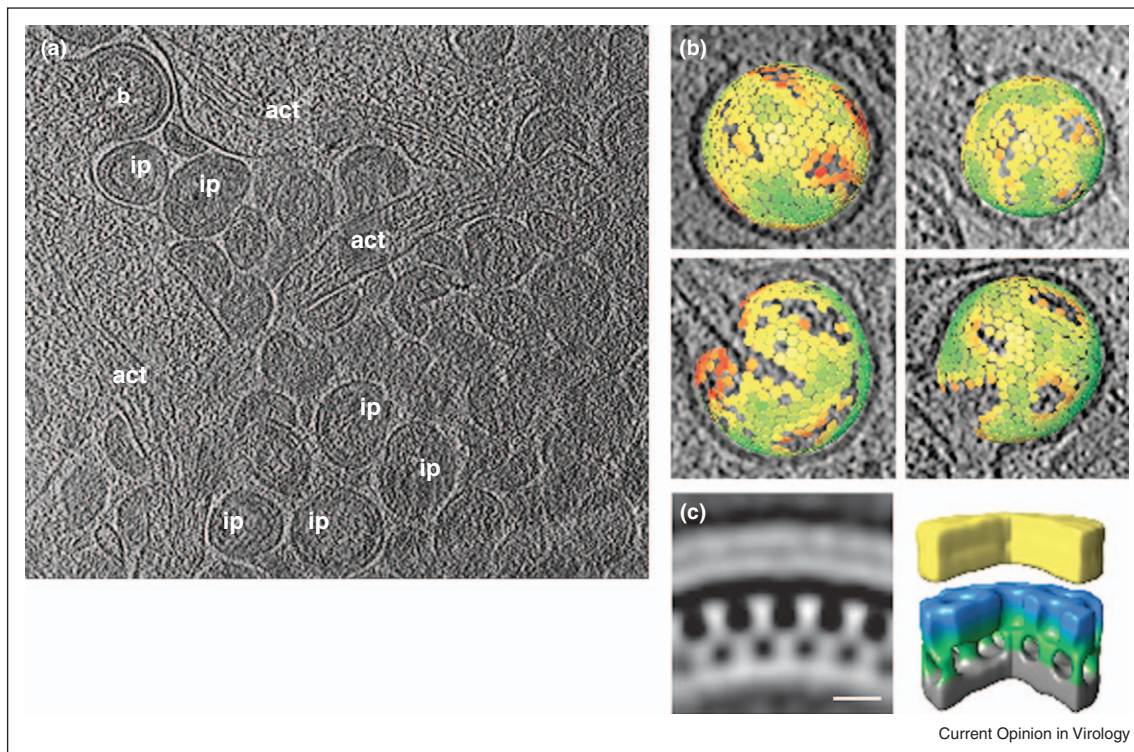
Cryoelectron tomography of HIV-1 budding sites and the gag protein lattice of the budding particles determined by sub tomographic averaging. **(a)** A computationally isolated tomographic slice of cells transduced with adenoviral vectors expressing HIV-1 Gag. act, actin; b, budding sites; ip, immature particles. **(b)** Gag lattice maps of immature (top) and intermediate (bottom) HIV-1. The center and orientation of each aligned sub tomogram are marked with a hexagon and are colored according to the cross correlation on a scale from low (red) to high (green). **(c)** The average of the aligned sub tomograms extracted from an individual budding site was displayed in the central radial sections from the structure (left) and in isosurface rendering of the structure (right). The surfaces have been colored radially to illustrate different domains in Gag: yellow — membrane + MA; blue/green — CA; gray — NC + RNA. Reproduced with permission from Ref [23••].

resulting in local membrane destabilization at the rear end of the virus. The study found that the increased vesiculation of the plasma membrane at the budding sites after prolonged infection resulted in releasing viruses with changes to spherical shapes, which are less infectious than the filamentous particles.

Herpesvirus

A number of members in Herpesviridae cause diseases and tumors, including varicella zoster virus, cytomegalovirus, Epstein–Barr virus, and Kaposi's sarcoma-associated herpesvirus. This DNA virus has an icosahedral capsid surrounded by an amorphous protein layer (tegument) and an envelope coated with glycoprotein spikes [27,28]. The entry process of herpes simplex viruses was caught in action in 3D [29]. Recently, the life cycle of murine gammaherpesvirus including viral attachment, entry, assembly, and egress were also revealed (Figure 2) [30••]. The study showed the transient process of incoming capsids injecting viral DNA through nuclear pore complexes and the process of nascent DNA being packaged into progeny capsids as a spool coaxial with the putative portal vertex. The work demonstrated that the intra-nuclear invagination of nuclear membranes is involved in the nuclear egress of herpes virus capsids.

Vaccinia virus

Vaccinia virus is a member of Poxviridae and has complicated assembly and maturation pathways that were studied by ET [31,32]. The precursor membrane of the virus is recruited by viral proteins to generate open membrane crescents that coalesce to form spheroid sacks that eventually form the envelope for the virus. The incorporation of the DNA leads to particles with a 'nucleoid' subsequent transformation into the mature virus. The latter stage involves an extreme rearrangement of the particle envelope in which the original recruiting viral gene products are lost. The entry of vaccinia virus into mammalian cells was also characterized by cryoto-mog and showed that viruses undergo distinct structural rearrangements of the core and its surface spikes as well as de-condensation of the viral DNA upon binding to the cell surface [33•].

## Sulfolobus turreted icosahedral virus (STIV)

STIV belongs to PRD1-Adeno viral lineage and infects the archaea *Sulfolobus* growing in boiling hot springs [34]. The structure of the major capsid protein (MCP) is conserved across three domains of life, from adenovirus, and vaccinia virus, to bacteriophage PRD1 [35]. The assembly process of this inner-membrane-containing virus was revealed in intact *Sulfolobus* cells by whole cell cryotomog (Figure 3) [36••]. The partially assembled particles were observed in which the curvature and protein-membrane layer spacing resemble those of fully assembled particles. These intermediates support the model of assembly in which the capsid shell and the membrane are tightly coupled by defined local inter-

Figure 2
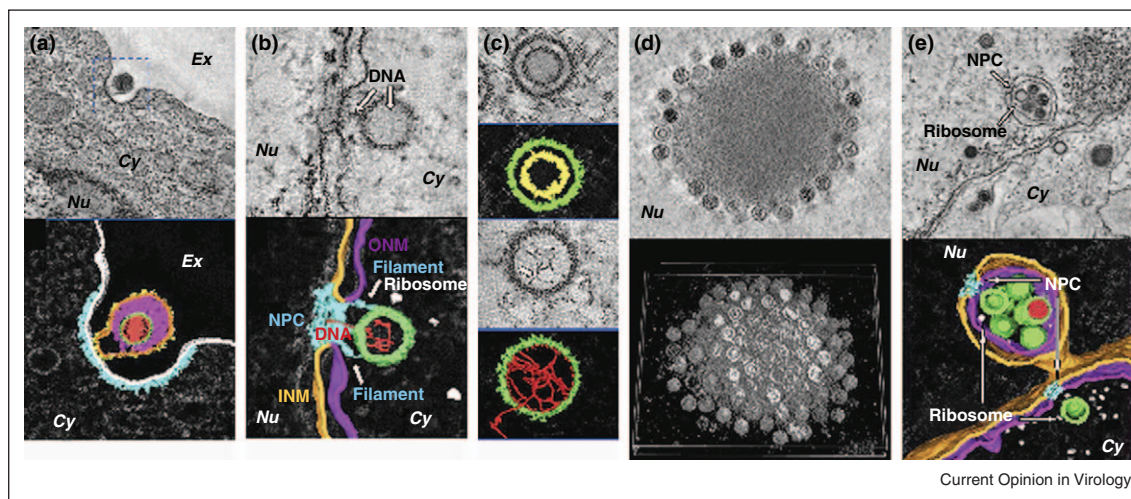
Dual-axis electron tomography of NIH 3T3 cells infected with murine gammaherpesvirus. **(a)** A tomogram (top) and the 3D rendering (bottom) of a virus attaching to the cell surface for prior to endocytosis. Color codes in 3D rendering: red, viral DNA; green, capsid; magenta, tegument; orange, envelope; yellow, protrusions on the membrane; light gray, plasma membrane; cyan, membrane coating. **(b)** A tomogram (top) and the 3D rendering (bottom) of a capsid docking at a nuclear pore and injecting viral DNA. Color codes in 3D rendering: red, viral DNA; green, capsid; light gray, ribosomes; orange, INM; magenta, ONM; cyan, NPC. **(c)** Tomograms (top) and the 3D rendering (bottom) of an assembly intermediate and a capsid packaging viral DNA. Color codes in 3D rendering: red, viral DNA; green, capsid; yellow, scaffolding protein. **(d)** A tomogram (top) and shaded surface views of entire sections of Virus-Induced Nuclear Inclusion Bodies. **(e)** A tomogram (top) and the 3D rendering (bottom) of capsids egressing from the nucleus. Color codes in 3D rendering: red, viral DNA; green, capsid; orange, INM or primary envelope; magenta, ONM or primary envelop in fusion; cyan, NPC; light gray, ribosome.Reproduced with permission from Ref [30••].

Figure 3
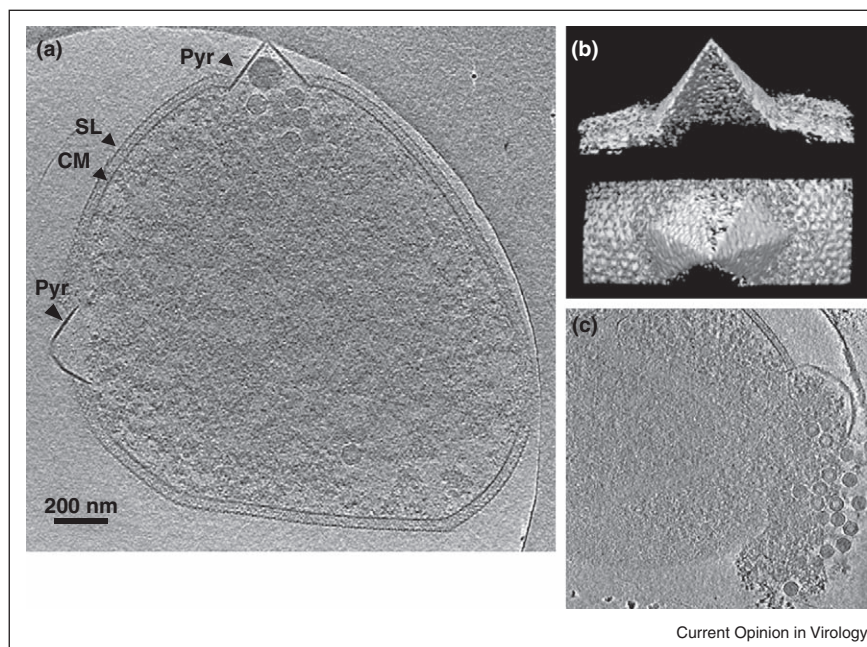
Whole cell cryoelectron tomography of *Sulfolubs* infected with STIV. **(a)** A computationally isolated tomographic slice of *Sulfolubs* infected with STIV. SL, s-layer; PS, periplasmic space; CM, cytoplasmic membrane; Pyr, pyramid-like protrusion; STIV, STIV particles. **(b)** Surface representations of a pyramid in 3D viewed from the side and the top of the structure. **(c)** A computationally isolated tomographic slice of *Sulfolubs* bursting out particles from a pyramid structure.
Reproduced with permission from Ref [36●●].

actions as assembly proceeds. Similar to the assembly of immature vaccinia viruses, the interactions of the lipid membrane with capsid, and possibly other trans-membrane proteins, appear able to maintain the energetically unfavorable open-ended membrane structures [31,32]. Indeed the high level of structural homology between the STIV MCP and the vaccinia D13 protein that recruits and shapes partially formed membrane structures is striking. This similarity in membrane recruiting subunits closely reveals comparable roles in STIV and vaccinia viruses but with different outcomes, that is STIV MCP forms membrane-containing viruses while vaccinia D13 is a scaffold that leaves the membrane during virus maturation and is not present in viruses (Figure 4). The power of cellular ET to disclose transient assembly and maturation intermediates, which may not be preserved in purified samples, is well illustrated by this example.

Sub tomographic reconstructions of the icosahedral particles allowed the structural comparison of particles *in situ* at various maturation stages [36●●,37]. The study clearly showed an empty precursor particle assumed to be the substrate for packaging enzymes analogous to bacteriophage. At the resolution of the sub tomographic reconstructions it did not appear that DNA packaging in STIV induced large-scale capsid transformation as observed in bacteriophage. It was clear that the turret-

like structures at the fivefold vertices seen in the mature viruses were already assembled in the procapsid particles before genome encapsidation. The high image quality of cellular tomograms and robust computational analysis allowed intracellular STIV arrays to be analyzed in exceptional detail, including the precise orientation of the particles within particle arrays. Particles in the arrays were packed tightly and mainly consisted of virions. Procapsids (lacking dsDNA) were only found on the edge of the arrays or not associated with the arrays at all. The arrays of STIV may accommodate DNA and packaging enzymes where capsid assembly and genome packaging are tightly coupled. Virus factories or viroplasm have been reported in eukaryotic and prokaryotic systems where proteins and newly synthesized genomes are confined within specific compartments for efficient viral replication and assembly [37–39]. The arrays observed in STIV may provide an environment for dsDNA packaging and maturation.

STIV infection induces the formation of pyramid-like protrusions on the cell surface that allow virus release late in infection [40,41]. A single viral protein was shown to induce pyramid formation even in the absence of virus infection [42,43]. Indeed, when this gene was expressed by itself in *Sulfolobus* pyramids formed on the cell surface. Fully developed pyramids have sevenfold symmetry and

Figure 4
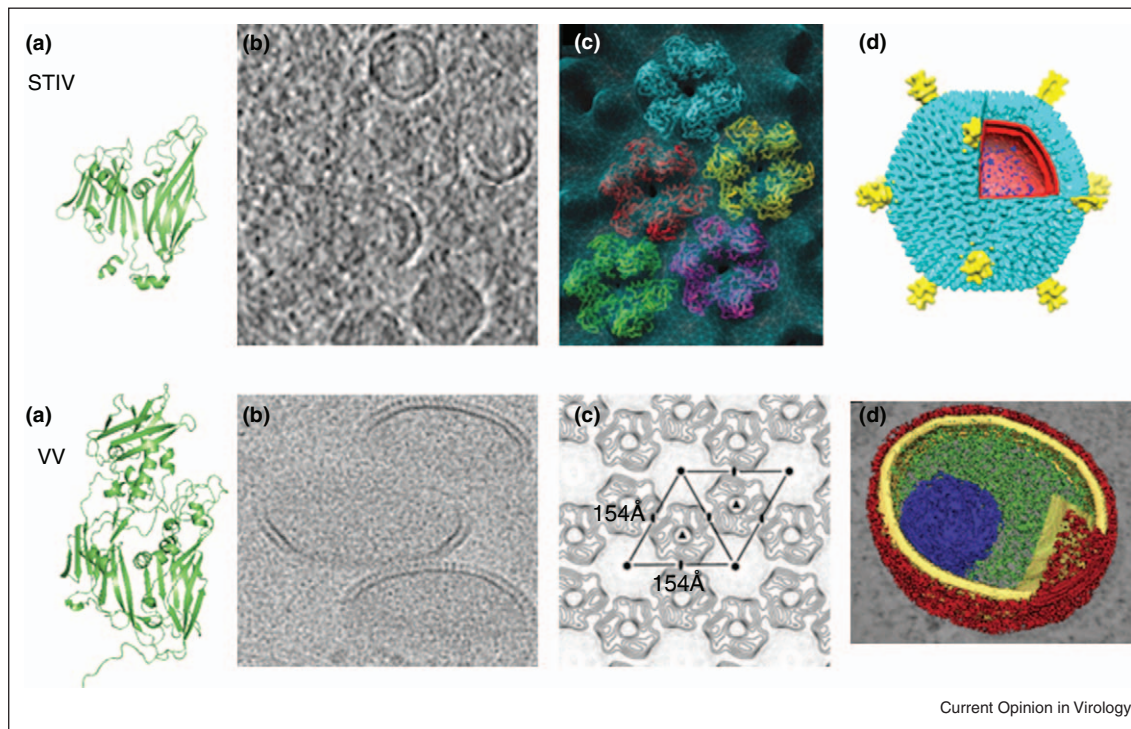
Hybrid approaches reveal conserved structures and assembly pathway of STIV and Vaccinia virus. The tertiary structures of the STIV MCP and Vaccinia virus D13 protein share similar folds **(a)** that recruit membranes to generate open membrane crescents **(b)** with hexagonal protein lattice packing **(c)**. The similar inner-membrane-containing particles are visualized **(d)**. Approximate scales for each panel are **(a)** STIV MCP ~37 kDa; VV D13 ~62 kDa. **(b)** STIV particle diameter ~74 nm; VV center diameter ~200 nm. **(c)** STIV hexamer center-to-center dimension ~74 Å; VV dimension ~154 Å. **(d)** STIV particle diameter ~75 nm; VV immature particle diameter ~270 nm (long axis). Reproduced with permission from Refs [32,35,54–56].

display sharp facets. Viewed perpendicular to the facets, the pyramids have a thicker cross-section than the cytoplasmic membrane and did not contain the exterior surface protein layer (S-layer). The process of pyramid protruding out of a thinning cell wall and perturbing the S-layer were captured by cryotomog, revealing exceptional detail associated with this novel viral release mechanism.

Conclusions

Cryotomog has evolved to visualize sophisticated virus life cycles and cellular pathogenesis in unprecedented detail. Employing multiple tilt procedures and more sophisticated programs to assemble the tomograms from individual images can reduce the missing wedge and correct for radiation damage to produce higher quality density. Direct electron detectors have recently been employed and appear to have great promise for improving signal to noise in cryo-EM imaging in general and cryotomog in particular [44]. Likewise, recent developments with Zernike phase-contrast cryotomog allowed the acquisition of images of unstained specimens with striking contrast while close to focus, allowing further improvement in resolution. Their use will benefit, in

particular, imaging ultrastructures of thick specimens under biological conditions [45,46].

Correlative fluorescence light microscopy and electron microscopy approaches have been developed employing fluorescent tags to guide the search for structures or events of interest followed by ET or cryotomog to provide high-resolution imaging of the biological events [47]. A similar rationale has driven the incorporation of the tetracysteine motif into a protein of interest. This motif induces fluorescence when it binds to biarsenical compounds (FlAsH and ReAsH) allowing specific targeting with light microscopy [48,49]. Following photo-conversion and osmium staining, an insoluble osmio-philic precipitate forms around the fluorescent target making it visible by EM. The approach was applied to follow the assembly of flock house virus in insect cells [50]. It allowed viral arrays to be visualized with both fluorescence and EM analysis and showed that heavily modified mitochondria were the sites of viral RNA replication. *In vivo* labeling strategies applicable to cryotomog have also developed recently. Metal-binding proteins such as metallothionein (MT) or ferritin can be fused to target proteins as can proteins that

will bind to gold clusters or heavy metal ions that can be visualized with EM [51–53]. Analogous to GFP used in fluorescence light microscopy, the metal-binding tags allow identification and localization of target proteins in the context of fine ultrastructures in tomograms.

There is an exceptional amount of activity in this arena with new approaches being reported on a regular basis. It seems clear that the recent insights into virus infection and pathogenesis are just the beginning of a new era in electron microscopy and structural virology.

Acknowledgements

References and recommended reading

Papers of particular interest, published within the period of review, have been highlighted as:

- • of special interest
- •• of outstanding interest

1. Lucic V, Forster F, Baumeister W: **Structural studies by electron tomography: from cells to molecules**. *Annu Rev Biochem* 2005, **74**:833-865.

2. Jensen GJ, Briegel A: **How electron cryotomography is opening a new window onto prokaryotic ultrastructure**. *Curr Opin Struct Biol* 2007, **17**:260-267.

3. Sosinsky GE, Crum J, Jones YZ, Lanman J, Smarr B, Terada M, Martone ME, Deerinck TJ, Johnson JE, Ellisman MH: **The combination of chemical fixation procedures with high pressure freezing and freeze substitution preserves highly labile tissue ultrastructure for electron tomography applications**. *J Struct Biol* 2008, **161**:359-371.

4. Al-Amoudi A, Norlen LP, Dubochet J: **Cryo-electron microscopy of vitreous sections of native biological cells and tissues**. *J Struct Biol* 2004, **148**:131-135.

5. Huiskonen JT, Hepojoki J, Laurinmaki P, Vaheri A, Lankinen H, Butcher SJ, Grunewald K: **Electron cryotomography of Tula hantavirus suggests a unique assembly paradigm for enveloped viruses**. *J Virol* 2010, **84**:4889-4897.

6. Noda T, Sagara H, Yen A, Takada A, Kida H, Cheng RH, Kawaoka Y: **Architecture of ribonucleoprotein complexes in influenza A virus particles**. *Nature* 2006, **439**:490-492.

7. Harris A, Cardone G, Winkler DC, Heymann JB, Brecher M, White JM, Steven AC: **Influenza virus pleiomorphy characterized by cryoelectron tomography**. *Proc Natl Acad Sci U S A* 2006, **103**:19123-19127.

8. Battisti AJ, Chu YK, Chipman PR, Kaufmann B, Jonsson CB, Rossmann MG: **Structural studies of Hantaan virus**. *J Virol* 2011, **85**:835-841.

9. Cardone G, Winkler DC, Trus BL, Cheng N, Heuser JE, Newcomb WW, Brown JC, Steven AC: **Visualization of the herpes simplex virus portal in situ by cryo-electron tomography**. *Virology* 2007, **361**:426-434.

10. Chang JT, Schmid MF, Rixon FJ, Chiu W: **Electron cryotomography reveals the portal in the herpesvirus capsid**. *J Virol* 2007, **81**:2065-2068.

11. Bostina M, Levy H, Filman DJ, Hogle JM: **Poliovirus RNA is released from the capsid near a twofold symmetry axis**. *J Virol* 2011, **85**:776-783.

12. Chang JT, Schmid MF, Haase-Pettingell C, Weigele PR, King JA, Chiu W: **Visualizing the structural changes of bacteriophage Epsilon15 and its Salmonella host during infection**. *J Mol Biol* 2010, **402**:731-740.

13. Lee KK: **Architecture of a nascent viral fusion pore**. *EMBO J* 2010, **29**:1299-1311.

14. Subramaniam S, Bartesaghi A, Liu J, Bennett AE, Sougrat R: **Electron tomography of viruses**. *Curr Opin Struct Biol* 2007, **17**:596-602.

15. Grunewald K, Cyrklaff M: **Structure of complex viruses and virus-infected cells by electron cryo tomography**. *Curr Opin Microbiol* 2006, **9**:437-442.

16. Iwasaki K, Omura T: **Electron tomography of the supramolecular structure of virus-infected cells**. *Curr Opin Struct Biol* 2010, **20**:632-639.

17. Briggs JA, Riches JD, Glass B, Bartonova V, Zanetti G, Krausslich HG: **Structure and assembly of immature HIV**. *Proc Natl Acad Sci U S A* 2009, **106**:11090-11095.

18. Li S, Hill CP, Sundquist WI, Finch JT: **Image reconstructions of helical assemblies of the HIV-1 CA protein**. *Nature* 2000, **407**:409-413.

19. Ganser BK, Li S, Klishko VY, Finch JT, Sundquist WI: **Assembly and analysis of conical models for the HIV-1 core**. *Science* 1999, **283**:80-83.

20. Briggs JA, Grunewald K, Glass B, Forster F, Krausslich HG, Fuller SD: **The mechanism of HIV-1 core assembly: insights from three-dimensional reconstructions of authentic virions**. *Structure* 2006, **14**:15-20.

21. de Marco A, Muller B, Glass B, Riches JD, Krausslich HG, Briggs JA: **Structural analysis of HIV-1 maturation using cryo-electron tomography**. *PLoS Pathog* 2010, **6**:e1001215.

22. Carlson LA, Briggs JA, Glass B, Riches JD, Simon MN, Johnson MC, Muller B, Grunewald K, Krausslich HG: **Three-dimensional analysis of budding sites and released virus suggests a revised model for HIV-1 morphogenesis**. *Cell Host Microbe* 2008, **4**:592-599.

23. Carlson LA, de Marco A, Oberwinkler H, Habermann A, Briggs JA,
•• Krausslich HG, Grunewald K: **Cryo electron tomography of native HIV-1 budding sites**. *PLoS Pathog* 2010, **6**:e1001173.
The cryo-tomog studies of intact plunge-frozen human cells showed that the HIV assembling in the native budding sites had the similar gag lattice packing as that of the released immature virion. Losing control of proteolytic maturation led to the formation of aberrant particles.

24. Felts RL, Narayan K, Estes JD, Shi D, Trubey CM, Fu J, Hartnell LM, Ruthel GT, Schneider DK, Nagashima K *et al.*: **3D visualization of HIV transfer at the virological synapse between dendritic cells and T cells**. *Proc Natl Acad Sci U S A* 2010, **107**:13336-13341.

25. Sougrat R, Bartesaghi A, Lifson JD, Bennett AE, Bess JW, Zabransky DJ, Subramaniam S: **Electron tomography of the contact between T cells and SIV/HIV-1: implications for viral entry**. *PLoS Pathog* 2007, **3**:e63.

26. Welsch S, Kolesnikova L, Krahling V, Riches JD, Becker S,
• Briggs JA: **Electron tomography reveals the steps in filovirus budding**. *PLoS Pathog* 2010, **6**:e1000875.
Tomography studies revealed the budding process of the highly infectious filamentous filoviruses and correlated the increased vesiculation of plasma membranes at the budding sites to the budding of spherical particles with low infectivity.

27. Deng B, O'Connor CM, Kedes DH, Zhou ZH: **Cryo-electron tomography of Kaposi's sarcoma-associated herpesvirus capsids reveals dynamic scaffolding structures essential to capsid assembly and maturation**. *J Struct Biol* 2008, **161**:419-427.

28. Grunewald K, Desai P, Winkler DC, Heymann JB, Belnap DM, Baumeister W, Steven AC: **Three-dimensional structure of herpes simplex virus from cryo-electron tomography**. *Science* 2003, **302**:1396-1398.

29. Maurer UE, Sodeik B, Grunewald K: **Native 3D intermediates of membrane fusion in herpes simplex virus 1 entry**. *Proc Natl Acad Sci U S A* 2008, **105**:10559-10564.

30. Peng L, Ryazantsev S, Sun R, Zhou ZH: **Three-dimensional
•• visualization of gammaherpesvirus life cycle in host cells by
electron tomography**. *Structure* 2010, **18**:47-58.
The studies revealed the life cycle of murine gammaherpesvirus including
viral attachment, entry, assembly, and egress in host cells in 3D.

31. Chichon FJ, Rodriguez MJ, Risco C, Fraile-Ramos A,
Fernandez JJ, Esteban M, Carrascosa JL: **Membrane
remodelling during vaccinia virus morphogenesis**. *Biol Cell*
2009, **101**:401-414.

32. Chlanda P, Carbajal MA, Cyrklaff M, Griffiths G, Krijnse-Locker J:
**Membrane rupture generates single open membrane sheets
during vaccinia virus assembly**. *Cell Host Microbe* 2009,
6:81-90.

33. Cyrklaff M, Linaroudis A, Boicu M, Chlanda P, Baumeister W,
• Griffiths G, Krijnse-Locker J: **Whole cell cryo-electron
tomography reveals distinct disassembly intermediates of
vaccinia virus**. *PLoS One* 2007, **2**:e420.
The cryo-tomog studies characterized the disassembly and structural
rearrangements of vaccinia virus upon entering intact mammalian cells.

34. Ortmann AC, Wiedenheft B, Douglas T, Young M: **Hot
crenarchaeal viruses reveal deep evolutionary connections**.
Nat Rev Microbiol 2006, **4**:520-528.

35. Khayat R, Tang L, Larson ET, Lawrence CM, Young M,
Johnson JE: **Structure of an archaeal virus capsid protein
reveals a common ancestry to eukaryotic and bacterial
viruses**. *Proc Natl Acad Sci U S A* 2005, **102**:18944-18949.

36. Fu CY, Wang K, Gan L, Lanman J, Khayat R, Young MJ,
•• Jensen GJ, Doerschuk PC, Johnson JE: **In vivo assembly of an
archaeal virus studied with whole-cell electron
cryotomography**. *Structure* 2011, **18**:1579-1586.
The cryotomog studies revealed the life cycle of STIV in the context of the
whole cell and characterized pyramidal structures formed by the cellular
membrane that penetrated the S-layer in response to viral infection.

37. Netherton C, Moffat K, Brooks E, Wileman T: **A guide to viral
inclusions, membrane rearrangements, factories, and
viroplasm produced during virus replication**. *Adv Virus Res*
2007, **70**:101-182.

38. Bravo A, Serrano-Heras G, Salas M: **Compartmentalization of
prokaryotic DNA replication**. *FEMS Microbiol Rev* 2005,
29:25-47.

39. Cook PR: **The organization of replication and transcription**.
Science 1999, **284**:1790-1795.

40. Brumfield SK, Ortmann AC, Ruigrok V, Suci P, Douglas T, Young MJ:
**Particle assembly and ultrastructural features associated with
replication of the lytic archaeal virus sulfolobus turreted
icosahedral virus**. *J Virol* 2009, **83**:5964-5970.

41. Ortmann AC, Brumfield SK, Walther J, McInnerney K, Brouns SJ,
van de Werken HJ, Bothner B, Douglas T, van de Oost J,
Young MJ: **Transcriptome analysis of infection of the archaeon
Sulfolobus solfataricus with Sulfolobus turreted icosahedral
virus**. *J Virol* 2008, **82**:4874-4883.

42. Snyder JC, Brumfield SK, Peng N, She Q, Young MJ: **Sulfolobus
Turreted Icosahedral Virus c92 protein responsible for
formation of pyramid-like cellular lysis structures**.
J Virol, 85: 6287-6292.

43. Quax TE, Lucas S, Reimann J, Pehau-Arnaudet G, Prevost MC,
Forterre P, Albers SV, Prangishvili D: **Simple and elegant design
of a virion egress structure in Archaea**. *Proc Natl Acad Sci U S A*
2011, **108**:3354-3359.

44. Milazzo AC, Moldovan G, Lanman J, Jin L, Bouwer JC,
Klienfelder S, Peltier ST, Ellisman MH, Kirkland AI, Xuong NH:
**Characterization of a direct detection device imaging camera
for transmission electron microscopy**. *Ultramicroscopy* 2010,
110:744-747.

45. Fukuda Y, Fukazawa Y, Danev R, Shigemoto R, Nagayama K:
**Tuning of the Zernike phase-plate for visualization of detailed
ultrastructure in complex biological specimens**. *J Struct Biol*
2009, **168**:476-484.

46. Murata K, Liu X, Danev R, Jakana J, Schmid MF, King J,
Nagayama K, Chiu W: **Zernike phase contrast cryo-electron
microscopy and tomography for structure determination at
nanometer and subnanometer resolutions**. *Structure* 2010,
18:903-912.

47. Plitzko JM, Rigort A, Leis A: **Correlative cryo-light microscopy
and cryo-electron tomography: from cellular territories to
molecular landscapes**. *Curr Opin Biotechnol* 2009, **20**:83-89.

48. Gaietta G, Deerinck TJ, Adams SR, Bouwer J, Tour O, Laird DW,
Sosinsky GE, Tsien RY, Ellisman MH: **Multicolor and electron
microscopic imaging of connexin trafficking**. *Science* 2002,
296:503-507.

49. Sosinsky GE, Giepmans BN, Deerinck TJ, Gaietta GM,
Ellisman MH: **Markers for correlated light and electron
microscopy**. *Methods Cell Biol* 2007, **79**:575-591.

50. Lanman J, Crum J, Deerinck TJ, Gaietta GM, Schneemann A,
Sosinsky GE, Ellisman MH, Johnson JE: **Visualizing flock house
virus infection in Drosophila cells with correlated
fluorescence and electron microscopy**. *J Struct Biol* 2008,
161:439-446.

51. Mercogliano CP, DeRosier DJ: **Concatenated metallothionein
as a clonable gold label for electron microscopy**. *J Struct Biol*
2007, **160**:70-82.

52. Diestra E, Fontana J, Guichard P, Marco S, Risco C: **Visualization
of proteins in intact cells with a clonable tag for electron
microscopy**. *J Struct Biol* 2009, **165**:157-168.

53. Wang Q, Mercogliano CP, Lowe J: **A ferritin-based label for
cellular electron cryotomography**. *Structure* 2011, **19**:147-154.

54. Bahar MW, Graham SC, Stuart DI, Grimes JM: **Insights into the
evolution of a complex virus from the crystal structure of
vaccinia virus D13**. *Structure*, in press.

55. Hyun JK, Coulibaly F, Turner AP, Baker EN, Mercer AA, Mitra AK:
**The structure of a putative scaffolding protein of immature
poxvirus particles as determined by electron microscopy
suggests similarity with capsid proteins of large icosahedral
DNA viruses**. *J Virol* 2007, **81**:11075-11083.

56. Khayat R, Fu CY, Ortmann AC, Young MJ, Johnson JE: **The
architecture and chemical stability of the archaeal sulfolobus
turreted icosahedral virus**. *J Virol* 2010, **84**:9575-9583.

57. Leo-Macias A, Katz G, Wei H, Alimova A, Katz A, Rice WJ,
Diaz-Avalos R, Hu GB, Stokes DL, Gottlieb P: **Toroidal surface
complexes of bacteriophage varphi12 are responsible for
host-cell attachment**. *Virology*, 414: 103-109.

58. Nemecek D, Heymann JB, Qiao J, Mindich L, Steven AC: **Cryo-
electron tomography of bacteriophage phi6 procapsids
shows random occupancy of the binding sites for RNA
polymerase and packaging NTPase**. *J Struct Biol* 2010,
171:389-396.

59. Liu X, Zhang Q, Murata K, Baker ML, Sullivan MB, Fu C,
Dougherty MT, Schmid MF, Osburne MS, Chisholm SW *et al.*:
**Structural changes in a marine podovirus associated with
release of its genome into Prochlorococcus**. *Nat Struct Mol Biol*
2010, **17**:830-836.

60. Dai W, Hodes A, Hui WH, Gingery M, Miller JF, Zhou ZH: **Three-
dimensional structure of tropism-switching Bordetella
bacteriophage**. *Proc Natl Acad Sci U S A* 2010, **107**:4347-4352.

61. Neuman BW, Kiss G, Kunding AH, Bhella D, Baksh MF, Connelly S,
Droese B, Klaus JP, Makino S, Sawicki SG *et al.*: **A structural
analysis of M protein in coronavirus assembly and
morphology**. *J Struct Biol* 2011, **174**:11-22.

62. Gangodkar S, Jain P, Dixit N, Ghosh K, Basu A: **Dengue virus-
induced autophagosomes and changes in endomembrane
ultrastructure imaged by electron tomography and whole-
mount grid-cell culture techniques**. *J Electron Microsc (Tokyo)*
2010, **59**:503-511.

63. Keller PW, Adamson CS, Heymann JB, Freed EO, Steven AC: **HIV-
1 maturation inhibitor bevirimat stabilizes the immature Gag
lattice**. *J Virol* 2011, **85**:1420-1428.

64. White TA, Bartesaghi A, Borgnia MJ, Meyerson JR, de la Cruz MJ,
Bess JW, Nandwani R, Hoxie JA, Lifson JD, Milne JL *et al.*:
Molecular architectures of trimeric SIV and HIV-1 envelope

glycoproteins on intact viruses: strain-dependent variation in quaternary structure. *PLoS Pathog* 2010, **6**:e1001249.

65. de Marco A, Davey NE, Ulbrich P, Phillips JM, Lux V, Riches JD, Fuzik T, Ruml T, Krausslich HG, Vogt VM *et al.*: **Conserved and variable features of Gag structure and arrangement in immature retrovirus particles**. *J Virol* 2010, **84**: 11729-11736.

66. Butan C, Lokhandwala PM, Purdy JG, Cardone G, Craven RC, Steven AC: **Suppression of a morphogenic mutant in Rous sarcoma virus capsid protein by a second-site mutation: a cryoelectron tomography study**. *J Virol* 2010, **84**:6377-6386.

67. Chen J, Sun J, Atanasov I, Ryazantsev S, Zhou ZH: **Electron tomography reveals polyhedrin binding and existence of both empty and full cytoplasmic polyhedrosis virus particles inside infectious polyhedra**. *J Virol* 2011, **85**:6077-6081.

68. Soonsawad P, Xing L, Milla E, Espinoza JM, Kawano M, Marko M, Hsieh C, Furukawa H, Kawasaki M, Weerachatyanukul W *et al.*: **Structural evidence of glycoprotein assembly in cellular membrane compartments prior to Alphavirus budding**. *J Virol* 2010, **84**:11145-11151.

69. Fontana J, Lopez-Iglesias C, Tzeng WP, Frey TK, Fernandez JJ, Risco C: **Three-dimensional structure of Rubella virus factories**. *Virology* 2010, **405**:579-591.